Exploratory growth in the Li2MoO4-MoO3 system for the next crystal generation of heat-scintillation cryogenic bolometers

Matias Velázquez, Philippe Veber, Meryem Moutatouia, Pierre de Marcillac, Andrea Giuliani, Pia Loaiza, Dominique Denux, Rodolphe Decourt, Hassan El Hafid, Matthias Laubenstein, et al.

Exploratory growth in the Li_2MoO_4-MoO_3 system for the next crystal generation of heat-scintillation cryogenic bolometers

Matias Velázquez[a], Philippe Veber[a], Meryem Moutatouia[a], Pierre de Marcillac[b], Andrea Giuliani[b], Pia Loaiza[c], Dominique Denux[a], Rodolphe Decourt[a], Hassan El Hafid[d], Matthias Laubenstein[e], Stefanos Marnieros[b], Claudia Nones[f], Valentina Novati[b], Emiliano Olivieri[b], Denys V. Poda[b,g], Anastasiia S. Zolotarova[b,g]

[a] CNRS, Université de Bordeaux, ICMCB, UPR 9048, 87 avenue du Dr. A. Schweitzer, 33608 Pessac Cedex, France
[b] Centre de Sciences Nucléaires et de Sciences de la Matière, CSNSM, UMR 8609, CNRS-IN2P3-Université Paris-Saclay, Bât. 108, 91405, Orsay Campus, France
[c] Laboratoire de l'Accélérateur Linéaire, LAL, Université Paris Sud, CNRS/IN2P3, Université Paris-Saclay, F-91405 Orsay, France
[d] Faculté des Sciences Semlalia, Université Caddy Ayyat, Marrakech, Morocco
[e] Istituto Nazionale di Fisica Nucleare, Laboratori Nazionali del Gran Sasso, INFN-LNGS, I-67100 Assergi (AQ), Italy
[f] CEA Saclay, DSM/IRFU, 91191 Gif-sur-Yvette Cedex, France
[g] Institute for Nuclear Research, MSP 03680 Kyiv, Ukraine

Abstract

In this work, we report on the Czochralski growth of Li_2MoO_4 crystals up to 230 g for heat-scintillation cryogenic bolometers likely to be used in astroparticle physics and neutron spectroscopy. Their transmission properties, radiopurity levels and detector behavior characterizations were carried out in order to validate the crystal growth process. The melting characteristics, the partition coefficients of a broad range of impurities, the thermal expansion (lattice parameters and dilatometry) and specific heat properties of the crystals were measured, over a broad temperature range for the last two, providing new data likely to be used in crystal growth process numerical simulations. We also investigated the crystal growth of $Li_4Mo_5O_{17}$ and determined its melting behavior and specific heat. The physical properties directly relevant to heat-scintillation cryogenic bolometers of Li_2MoO_4 and $Li_4Mo_5O_{17}$ are discussed in the context of the current materials developed for such applications.

1. Introduction

The search for the neutrino mass and the direct detection of the dark matter of our universe stand among the most exciting science drivers of today's astroparticle physics, which also have strong implications in the realm of cosmology. Crucial experiments in these domains require detecting extremely rare events, such as neutrinoless double-beta decays (0v-DBD) [1], or direct searches for dark matter in the form of weakly interacting massive particles (WIMPs) [2]. The 0v-DBD is a rare nuclear process in which an isobar transforms into a lighter one emitting only two elecrons. If observed, this decay would prove that the neutrino is a Majorana particle, i.e a fermion equal to its own anti-fermion: a new type of matter. The implications of this fact would be far-reaching in fundamental physics, ranging from the understanding of the elementary particle masses to the explanation of the dominance of matter over anti-matter in the Universe. 0v-DBD will also give unique information about the neutrinos absolute mass scale. The direct detection of WIMPs would solve the recurring enigma on the nature of dark matter, which is expected to constitute 26% of our universe's content. Another emerging frontier research field where crystal-based heat-scintillation cryogenic bolometers (HSCBs) could also be successfully employed is the study of solar axions [3–5], hypothetical particles providing an elegant solution of the so-called "strong CP problem" in quantum chromodynamics (QCD) [6]. Last but not least, a major by-product of this research is the detection and spectroscopy of fast and extremely rare neutrons, which not only help understanding the ultimate background of the dark matter direct detection underground sites, but is *per se* a promising frontier research field for environmental issues. In all these cases,

because of their higher energy resolution, powerful particle identification ability and low energy threshold, HSCBs turn out to be very sensitive tools to carry out this exploratory research. HSCBs, which have significantly matured since their proposal in 1989 [7,8], work at very low temperature (≤25 mK) and measure an energy release in a single crystal by means of both heat and light pulses resulting from the same nuclear event. Their complementarity often allows for establishing the nature of the incident particle and consequently for rejecting the radioactivity background, which is mandatory when the signal rate is vanishingly small. As compared with detectors based on noble liquids, which exploit self-shielding to reject the background, HSCBs rely on their superior energy resolution and discrimination power. High energy resolution particle detectors containing Mo as a constituent element have a tremendous potential in fundamental neutrino physics, especially if the detectors can be made with an extremely low content of radioactive impurities and if they are capable to tag alpha events. The reason is that the isotope ^{100}Mo, present at the 9.7% level in natural molybdenum, is an excellent candidate for a rare nuclear process known as 0v-DBD.

The core of HSCBs is made of radiopure bulk single crystals constituted as much as possible of nuclei that exhibit high capture cross sections of the relevant particles or that are themselves the source of the rare event to be detected. It just so happens that Li_2MoO_4, because of the possibility to be enriched with ^{6}Li, ^{7}Li or ^{100}Mo isotopes, of the absence of long-lived radioactive isotopes (such as ^{48}Ca and ^{113}Cd, harmful for cryogenic 0v-DBD searches), its remarkable ^{232}Th and ^{238}U chains radiopurity, of its high Mo-weight proportion (55%), of its reasonable light yield at low temperatures (≈1 keV/MeV), of its low and congruent melting point (it has been widely used as a solvent for the growth of many refractory oxide crystals), is a strategic crystal likely to satisfy the requirements for no less than three types of rare events detection: 0v-DBD, fast neutron backgrounds and solar axions. It is thus necessary to develop the growth process of large and constant diameter Li_2MoO_4 single crystals, of mass in the range 350–500 g. This mass represents a reasonable compromise between keeping acceptably high amplitudes of the heat signals [9], and avoiding too small crystals, which would oblige to develop large arrays when a high total active mass is required, as in 0v-DBD search for example. More precisely, the calculations on the pile-up due to two-neutrino double-beta decay (2v-DBD) show that the maximum acceptable mass in Li_2MoO_4 is on the order of 350 g, and this mass value should be taken as a target [10]. These devices have very high energy resolution – a few keV – at the DBD signal (just a peak at the Q-value of the nuclear transition for a detector containing molybdenum), which is 3034 keV in the case of ^{100}Mo, i.e. outside the bulk of the natural gamma radioactivity. In addition, the simultaneous detection of heat and light which characterizes scintillating bolometers allows to separate beta events (potential signal) from alpha events (certain background, expected to be dominant in that energy region). Since alpha particles produce much less scintillating light than beta particles, for the same release of heat, this discrimination can be made. The ratio of the light-to-heat signal amplitudes represents therefore a safe discrimination index.

Li_2MoO_4 was studied at first as a promising material for HSCB operation in 2010 by using a small 1.3 g crystal sample [11]. Larger crystals were grown in 2013 by both our group and a group of the Mendeleyev University of Chemical Technology of Russia, in Moscow, who grew independently ~100 g Li_2MoO_4 crystals by the Czochralski technique under air in a Pt crucible at 4 mm/h [12]. Later on, a low quality 34 g Li_2MoO_4 (φ22 × 33 mm) single crystal was tested at the Laboratori Nazionali del Gran Sasso (LNGS) underground laboratory under bolometer operation (344 h background measurement) with quite encouraging results demonstrating that it is a viable candidate for 0v-DBD of ^{100}Mo, with prospects of neutron spectroscopy thanks to the exothermic ^{6}Li(n,t)α reaction (Q = 4.78 MeV) and good intrinsic radiopurity levels. However, it is worth noting that the test of the material radiopurity level carried out before the bolometric test by means of ultra-low background HPGe (high-purity Ge detector) gamma spectrometry at LNGS revealed a considerably high ^{40}K-content at the level of 0.2 Bq/kg. The envisioned large mass of the crystals and the possibility to develop large arrays of these devices could also set the basis for a ^{7}Li solar

axion search [4,5] with unprecedented sensitivity. The first test of the material radiopurity level was carried out by means of ultra-low background HPGe gamma spectrometry at the LNGS laboratory [13]. Then, Li_2MoO_4 crystals with diameter ≈5 cm were grown by the Czochralski method [14]. In late 2014, medium volume Li_2MoO_4 crystals were developed in Nikolaev Institute of Inorganic Chemistry (NIIC, Novosibirsk, Russia), from deeply purified molybdenum by using the low-temperature-gradient Czochralski method. Aboveground cryogenic tests of a 151 g crystal allowed to estimate preliminarily its radiopurity level, providing much stronger elements for their convenient use in DBD search [15], and to ascertain that Li_2MoO_4-based HSCBs are excellent instruments for neutron detection. Indeed, a low-temperature test of a scintillating bolometer based on a Li_2MoO_4 cylindrical crystal (Ø = 40 mm and h = 40 mm) was performed at ~15 mK during several days in an aboveground pulse-tube cryostat housing a high-power dilution refrigerator at CSNSM. These measurements demonstrated an excellent performance of the detector in terms of both energy resolution and α/ß separation power. The size of the scintillating bolometer was at least 5 times higher than that of any previously operated device based on Li_2MoO_4, and it is not far from the volume required for the single module of a large array to be used in a competitive 0v-DBD experiment.

In Ref. [16], and in plenty of subsequent works, Li_2MoO_4 is often mentioned as a useful eutectic former for the flux growth of many refractory oxides, and indeed, it was investigated as such. It has a low congruent melting point, with T_m ≈ 710 °C and ΔS_m ≈ 6 R [17], a liquid viscosity at such temperature η(710 °C) ≈ 8 cP and a liquid volumic mass ρ ≈ 2.66 g cm^{-3}.

In this work, we present the Czochralski growth of ≈230 g Li_2MoO_4 crystals as a significant step towards the realization of the future 0v-DBD and fast neutrons detectors. The crystals were characterized from the viewpoint of the HSCB application, which requires as low as possible specific heat and as high as possible thermal conductivity at cryogenic temperatures, or high Debye temperature (θ_D > 500 K), the absence of thermoluminescence and a strong emission in the 400–1700 nm spectral range and extremely high radiopurity levels, especially here in terms of K concentration (which is an alkaline earth like Li). These requirements must be fulfilled by the crystals if a large mass of them are to be cooled down 20 mK and less, and if large light/heat discrimination ratio are to be obtained for a better efficiency of the detector. We also present exploratory results of $Li_4Mo_5O_{17}$ crystal growth and related characterizations.

2. Experimental procedures

2.1. Thermodynamic stability, Czochralski growth of Li_2MoO_4 bulk crystals and chemical trace analysis of the raw materials

The initial charge for growing single crystals was prepared starting from the following raw materials: 5N5 MoO_3 powder from Alfa Aesar and 5N Li_2CO_3 powder. Li_2CO_3 and MoO_3 were weighed in stoichiometric amounts and mechanically mixed. The stoichiometric mixture was thermally treated in air in successive stages at 400 °C for 12 h and 600 °C for 24 h, separated by intermediate grindings. Due attention was paid not to volatilize unreacted MoO_3 starting product. In one of the crystal growth run, 4N Eu_2O_3 powder was added to the initial mixture (Eu:Mo ~ 1/1000) in order to try to dissolve a few ppm of Eu^{3+} cations in the final crystal and make it scintillate more efficiently. The phase purity of the final products was determined by powder X-ray diffraction. The growth was carried out in a Pt crucible and in air atmosphere on approximately [110]-oriented Li_2MoO_4 single crystal seed, at temperatures maintained below 720 °C to minimize Li_2MoO_4 bath chemical decomposition and subsequent MoO_3 volatilization. Slow pulling and crystal rotation rates were applied (0.6 mm/h and 5 rpm) and the average mass uptake was ~3.5 g/h in axial and radial thermal gradients which could not be measured precisely

but were at least 20 °C/cm. Thermal insulation all around the Pt crucible and the position adjustment of the latter were insured by means of zirconia supports and mm-sized balls, mounted with two alumina rods (5–8 mm in thickness). After completion of the growth the cooling rate was 3.7 °C/h. Neither reduction nor volatilization during the synthesis and growth ($P_v(MoO_3$, 1000 K) = 1.4 × 10^{-3} atm) were observed. The crystals are hygroscopic and must be stored in a dried environment otherwise their surface becomes opaque after several weeks of exposure to air, and eventually gets liquefied. Several crystals were grown, each weighing at least one hundred grams, with crystallization yields ranging from 43 to 56%. They are colourless, transparent, and the crystal shown in Fig. 1 does not exhibit facets nor cleavage planes. Exhaustive glow-discharge mass spectrometry (GDMS) chemical trace analysis was performed on the starting powders. The 5N5 commercial MoO_3 powder was found to contain less than 0.05 ppm of Zn, 0.46 ppm of Mg, 0.55 ppm of K, 2 ppm of Si, 2.8 ppm of Fe, 4.8 ppm of Ca, 6.3 ppm of Na and 49 ppm of W. The upper bound that could be put on the U and Th concentrations was found to be 3 ppb, and that on Ra concentration 1 ppb. Hence, our initial MoO_3 powder is purer than the doubly sublimed and recrystallized from aqueous solution MoO_3 powder used in Ref. [18], in terms of K, Si, Fe and Zn concentrations, equally pure in terms of Mg and Ca concentrations, and less pure in terms of Na and W concentrations. Note that our initial MoO_3 powder is not the one mentioned in tables 2 and 3 of Ref. [18]. The 5N Li_2CO_3 powder was found to contain less than 0.1 ppm of Zn, 0.06 ppm of Mg, 0.32 ppm of K, 1.3 ppm of Si, 0.22 ppm of Fe, 0.94 ppm of Ca, 0.43 ppm of Na and less than 0.05 ppm of W. The upper bound that could be put on the U, Th and Ra concentrations was found to be 1 ppb. In addition, the radioactive contamination of 300 g of the lithium carbonate powder was measured with the help of a high purity Ge detector at the STELLA facility at LNGS (Italy) [19]. The results demonstrate that the bulk ^{40}K activity is less than 35 mBq/kg, the activities of ^{228}Ra and ^{228}Th of the ^{232}Th decay chain were found to be 37 and 34 mBq/kg, respectively. In the ^{238}U decay chain, the ^{226}Ra activity amounted to 272 mBq/kg.

Fig. 1. A 230.54 g [110]-oriented Li_2MoO_4 crystal (h = 6 cm, average φ = 4 cm) grown by the Czochralski method in the conditions described in Section 2.1.

2.2. Li_2MoO_4 physical properties measurements

The investigation on the Li_2MoO_4 melting point was performed by means of calorimetric measurements from 295 to 998 K, at a temperature variation rate of ß ≈ 6 °C/min ≈ 100 mK/s, with a commercial power compensation disk-type heat flux differential scanning calorimeter. A

flat single crystalline block of 53.835 mg was used, as well as three standards for the temperature and energy calibrations in Pt crucible under an O_2 flow.

The optical transmittance of the Li_2MoO_4 crystals was recorded from 200 to 3000 nm with a Varian Cary 5000-UV-vis-NIR spectrometer, and completed at higher wavelengths by measurements on a Bruker FT-IR spectrometer. The measurements were performed on [−1 0 –4]-oriented crystalline cubes of approximate thickness 10 mm (see Fig. 2), which permitted to calibrate the absorption spectra in cross section units. We used the data of ref. [20] to obtain a Sellmeier-type equation for the optical index between 407.7 and 579 nm, $n^2 = 1 + 0.0002\lambda^2/(\lambda^2 - 165392.32836) + 1.8677\lambda^2/(\lambda^2 - 17613.65559)$, and to estimate the absorption coefficient corrected for Fresnel reflection losses by extrapolation in the visible spectral range where the scintillation light is expected. Two crystalline cubes were cut from a bulk which had fallen into the growth load before its growth was completed. In none of these cubes could be found W, Ti, Na, Fe nor any other element at the 10–100 ppm level by Electron Probe Micro-Analysis/Wavelength Dispersion Spectroscopy analysis. One of this cube, cut from a seemingly defect-free single crystalline part, was clear and colourless, and the other one, cut from the very bottom part in the remaining growth load in the crucible, was faint yellow to the naked eye.

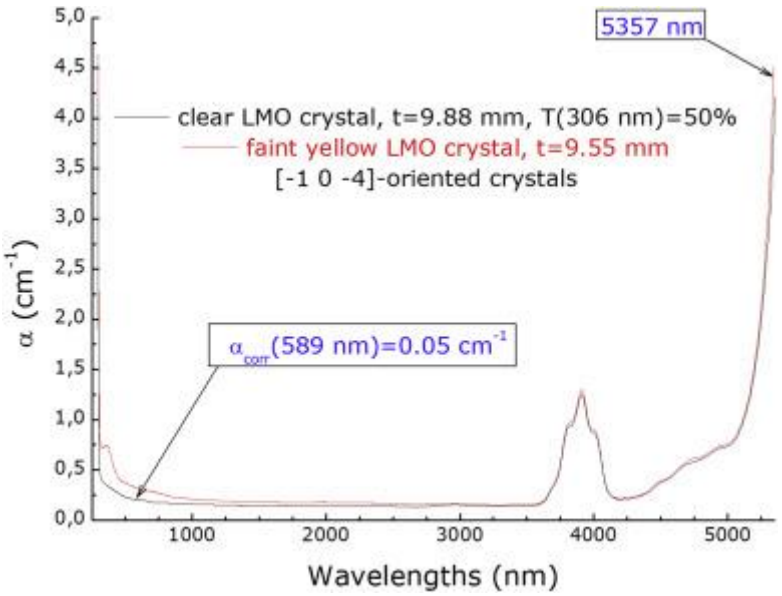

Fig. 2. Absorption coefficient of two Li_2MoO_4 crystals uncorrected for Fresnel reflection losses. α_{corr} means α corrected for Fresnel reflection losses by means of a Sellmeier-type equation determined from the optical index data given in Ref. [20]. The accuracy on α_{corr} is better than 1%.

The lattice parameters thermal expansion was determined by performing Le Bail fits of X-ray powder diffraction patterns with the crystallographic model of Ref. [21]. We performed powder X-ray diffraction (XRD) at 300, 250, 200, 150, 100 and 300 K again, in order to assess the reversibility of the process. The cooling was ensured by monitoring a He flux ranging from 0.5 L/h at room temperature to 2.5 L/h at low temperature. The data were collected in the Bragg-Brentano geometry with a 0.02° step at a rate of 0.24°/min. The high temperature measurements were performed in air with a first heating at 10 °C/min up to 600 °C, and then a measurement every 50 °C with a cooling rate 2 °C/min. The powder was sieved down to 63 µm.

The dilatometry measurements were performed by means of a differential dilatometer NETZSCH 402 ED, under an electronic grade Ar flux, from room temperature to 650 °C. The crystals used were oriented by the Laue method, cut along ***a*** and ***c***, and fixed on a Pt-protected alumina sample holder. Three heating-cooling cycles at a temperature variation rate of 1 °C/mn were performed, and only the last two ones were kept. Two strictly identical, in terms of size, sapphire crystals were used as standards in order to eliminate residual asymmetry effects during the experiments carried out on Li_2MoO_4 crystals.

The specific heat (C_p) measurements of the crystals were made between ~350 K and ~2 K in an adiabatic calorimeter using the relaxation technique supplied by a commercial heat capacity measurement system (Quantum Design, PPMS model). Single crystals with sizes of 3 × 3 × 1 mm^3 were mounted on an aluminum plate with apiezon grease for better thermal contact. LiF and α-Al_2O_3 crystals are standards which we used to calibrate our Debye temperature estimations since the Debye temperature of these two crystals is well established.

A 31.5 days run in the HPGe γ-spectrometer planar detector of the Laboratoire Souterrain de Modane (LSM) carried out with a 46 g Li_2MoO_4 crystal permitted to measure the activities summarized in Table 1.

A few-day low-temperature test of a scintillating bolometer based on a Li_2MoO_4 nearly cylindrical crystal (φ = 36–40 mm, h = 47.5 mm and m = 158 g) and a HPGe-based light detector (φ44 × 0.18 mm) was performed at ~18 mK in an aboveground pulse-tube cryostat housing a high-power dilution refrigerator in CSNSM (Orsay, France). Background and calibration (^{232}Th) measurements of 130 h data set were analyzed.

3. Results and discussion

During our growth experiments, we did not observe convection “cartwheels” in the dark yellow liquid, while the crystal remains colourless in the vicinity of the solidification interface. According to [21], the crystal structure adopts the R-3 space group with lattice parameters a = b = 14.34 Å, c = 9.593 Å and γ = 120°. In this structure, one can distinguish six crystallographically equivalent and unconnected between each other MoO_4^{2-} tetrahedra, all adopting the C_1 point group symmetry. The largest lattice spacings d_{hkl}'s can be listed by the following decreasing order: d_{-111} = 7.6 Å, d_{-120} = 7.2 Å, d_{021} = 5.2 Å, d_{012} = 4.5 Å, d_{-231} = d_{-321} = 4.2 Å. In all the crystals that we grew, only one facet formed once and was obviously a kinetic one (d_{131} = 3.24 Å) for it formed when the applied growth rate was 1.8 mm/h. This facet covered only a very small surface of a ~105 g crystal periphery. The low Jackson factor, the overall absence of faceting and the temperature dependence of the lattice expansion (Fig. 3) could be due to the activation of rotational degrees of freedom of MoO_4^{2-} tetrahedra, which are isolated from each other.

3.1. Differential scanning calorimetry (DSC) reinvestigation of the Li_2MoO_4 melting point

The DSC experiments were carried out in order to carefully establish the melting point of Li_2MoO_4 crystals, assess the congruent nature of the fusion, measure the melting enthalpy and estimate the minimum bound that can be set to the Jackson factor. The low supercooling of the melt makes it possible to use the low-temperature-gradient Czochralski method for these crystals. The melting onset temperature was determined to be T_m = (975.0 ± 1.0) K, and the melting enthalpy and entropy amount to ΔH_m = (49.66 ± 1.99) kJ/mol and ΔS_m = (6.13 ± 0.25) R, respectively. The melting entropy proves to be lower than that found in KPb_2Cl_5[22], in Tl_3PbBr_5[23], in Tl_3PbBr_5[24], in $PbFe_3O(PO_4)_3$[25], in $Li_6Eu(BO_3)_3$[26] and in $Ba_2LaFeNb_4O_{15}$[27]. All the latter crystal examples were grown with large facets. We performed a scrutinous examination of the crystal structure of

several Li_2MoO_4 planes, taking into account when one or several atoms were present in crystallographically nonequivalent sites, and found that the geometric factor could hardly take lower values than 0.5 for the (−121), (011) and (111) planes, and higher values than 0.75 for the (−120) plane, which means that in this crystal, a safe range of values ~3–4.5 can be put forward for the Jackson factor. 2D mean field theory predicts the occurrence of a surface roughening transition for a Jackson factor lower than $\alpha_C = 2$, whereas in the 2D and 3D Ising universality classes, a critical Jackson factor of 3.5 and 3.2 is found, respectively. Hence, owing to its low melting entropy, and a crystal structure which is not very compact, Li_2MoO_4 has a Jackson factor which lies within the range where roughening transitions with Ising-type critical behavior are expected.

Table 1
Radioactive contamination of the 46 g Li_2MoO_4 crystal cut out from the first produced ~104 g Li_2MoO_4 bulk crystal measured by HPGe γ-spectroscopy and of the advanced 158 g crystal cut from the large Li_2MoO_4 boule (shown in Fig. 1) and tested as a scintillating bolometer. Limits are given 95% c. l., uncertainties at 68% c. l.

Decay chain	Radionuclide	Bulk activity (mBq/kg) in Li_2MoO_4 crystals	
		46 g (HPGe, 31.5 days)	158 g (Scintillating bolometer, 130.4 h)
^{238}U	^{238}U	≤55	≤0.25
	^{226}Ra	2.6 ± 1.7	≤0.37
	^{210}Pb	≤462	–
	^{210}Po	–	1.41 ± 0.14
^{235}U	^{235}U	≤14	–
	^{227}Th	–	≤0.30
^{232}Th	^{232}Th	–	≤0.21
	^{228}Ra	≤13	–
	^{228}Th	≤4	≤0.27
	^{40}K	≤47	–

In this situation, if low-temperature-gradient Czochralski method is applied, at low growth rates, there will be a risk that rough and plane domains coexist at the solidification interface, with resulting impurity incorporation at the boundaries between these domains. It will be necessary to increase the growth rate to avoid impurity trapping, to select and tune the faceting, at the expense of the interface morphological stability and in favor of thermal stresses. Nevertheless, given the moderate amount of latent heat (for an ionic oxide), it should be feasible to increase the growth rate of Li_2MoO_4 up to 1.7 mm/h, which corresponds to a crystal mass uptake of 10 g/h, typical of an industrial production of 20 crystals per year per Czochralski puller, if a one ton 0v-DBD experiment is to be built someday.

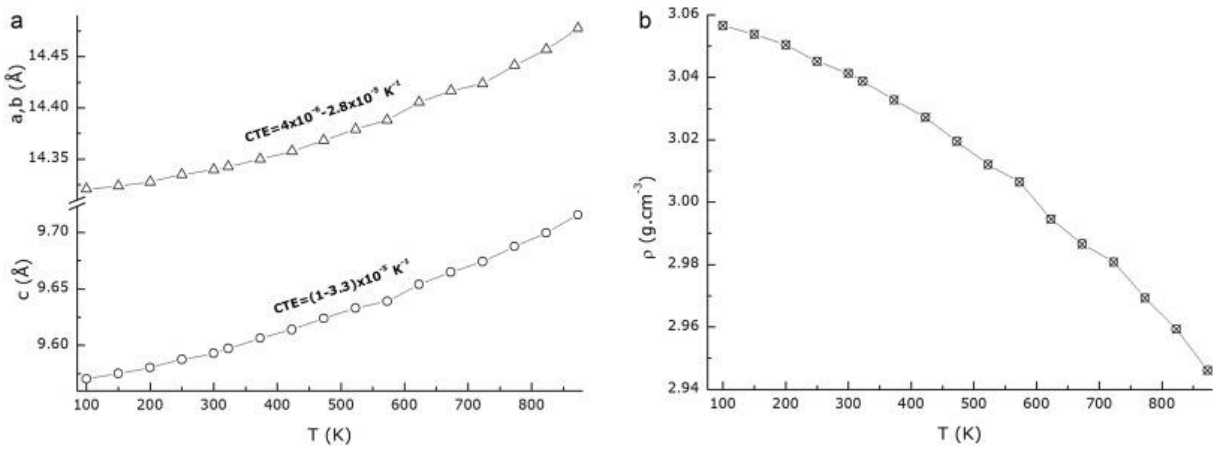

Fig. 3. Li_2MoO_4 lattice parameters thermal expansion between 100 and 873 K. Top: a and c (Å) versus T (K). Bottom: X-ray volumic mass (g/cm^3) versus T (K).

3.2. Li_2MoO_4 optical transmission

In Fig. 2, it turns out that the absorption coefficient of the clear and colourless crystal decays from 0.056 to 0.035 cm^{-1} between 550 and 670 nm. Such values are already close to the specifications required for a ton-scale 0v-DBD experiment ($\alpha_{corr} \sim 1/30\ cm^{-1}$). On the same spectral range, the absorption coefficient of the faint yellow crystal (mentioned in Section 2.2.) decreases from 0.191 to 0.147 cm^{-1}, that is, a factor of 3.4-4.2 with respect to the clear and colourless crystal.

3.3. Lattice parameters and volumic mass as a function of temperature

The data shown in Fig. 3 was found to fit with a second order polynomial. On average between 100 K and RT, the thermal contraction upon cooling is ≈ $-5.85\ 10^{-6}\ K^{-1}$ along ***a***, and ≈$-1.28\ 10^{-5}\ K^{-1}$ along ***c***, which leads to an average overall thermal contraction 2 to 3 times higher than that of $ZnMoO_4$, and ~1.4 times higher than that of Ge, the choice material for heat-ionization cryogenic bolometers [2]. It is important to take into account such a contraction in the design of the bolometer and to standardize all the cooling procedures during assembly and measurements campaigns. Extrapolating $\rho(T \rightarrow T_m)$ leads to a maximum estimate of $(\Delta\rho/\rho)_m \sim -9\%$ and a $\Delta V_{mol} \approx 5.61\ cm^3\ mol^{-1}$ at the melting point of Li_2MoO_4. The macroscopic thermal expansion was measured on crystallographically oriented Li_2MoO_4 crystals along ***a*** and ***c*** between room temperature and 923 K (≈0.94 T_m) and found to be completely reversible (Fig. 4). The remarkable point on Fig. 4 is that the lattice parameters thermal expansion curve virtually superposes on that of the crystal dilatation, up to 0.9 T_m. This means that there is no vacancy nor interstitial formation up to this temperature, and so no plastic flow nor creeping of the crystal is expected during solidification, or that there is a mutually compensating formation of both types of point defects leading to a completely reversible thermal expansion behavior, parabolic in temperature. Moreover, the overall thermal expansion in Li_2MoO_4 crystals prove to be rather small (~1.4%).

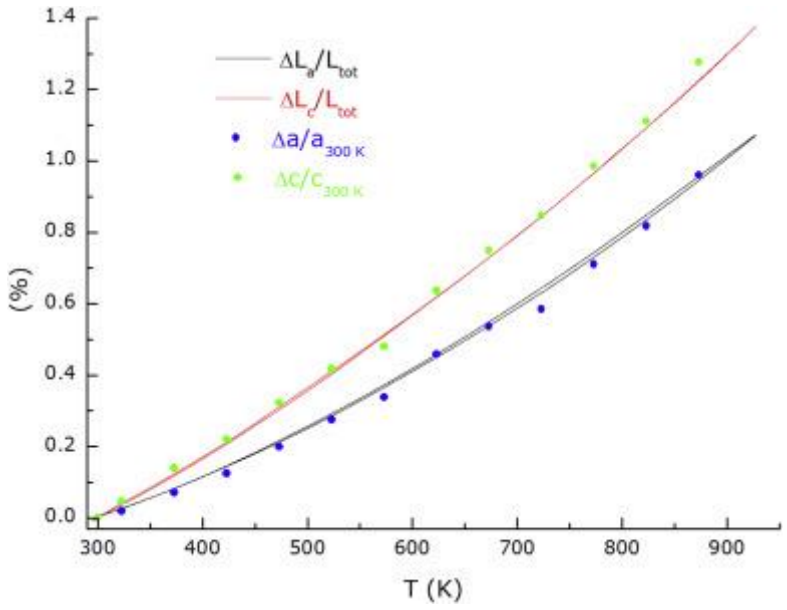

Fig. 4. Li_2MoO_4 lattice parameters thermal expansion and crystal macroscopic dilatation between room temperature and 923 K, along ***a*** and ***c*** directions. The error bars correspond approximately to the size of the points.

3.4. Gamma spectroscopy measurements and GDMS trace analysis

Exhaustive trace analysis performed by GDMS on pieces of the successive Li_2MoO_4 crystals that we grew evidenced an increase in K and Ba contaminations with crystal growth run number and with 4N Eu_2O_3 powder addition, as well as an increase in Ca and Fe contaminations with crystal growth run number. No such clear increase in Zr and W contaminations in time could be unveiled. The ^{40}K-activity shown in Table 1 (related to the 46 g crystal, which was cut out from a 104 g and first bulk crystal that we grew) are consistent with the GDMS analysis. The increase in K and Ba contamination with crystal growth run number and 4N Eu_2O_3 powder addition was correlated with an increase in ^{40}K and ^{226}Ra activity up to 4.4 ± 2.5 mBq/kg also measured by γ-spectroscopy. However, in the crystal shown in Fig. 1, the very low ^{226}Ra activity (≤0.37 mBq/kg) does not correlate with the Ba content of the crystal. Crystal scintillators containing rare-earth elements, in particular Ce and/or Gd elements (for instance, in Gd_2SiO_5, CeF_3 and $CeCl_3$), as well as Eu-doped scintillators like CaF_2:Eu, SrI_2:Eu and LiI:Eu, have been found to be strongly polluted, mainly by Th, but also by U [28–30]. A correlation between Ba content and Ra activity was recently established in a BaF_2 crystal [31]. Radium is well known as one of the most important radioactive contaminations in calcium containing crystals such as CaF_2:Eu [32], $CaWO_4$[33] and $CaMoO_4$[34].

The radioactivity level, estimated from the data of aboveground measurements at 18 mK with a ∼158 g Li_2MoO_4 crystal mounted as a scintillating bolometer was found to be very low: ^{232}Th ≤ 0.21 mBq/kg, ^{228}Th ≤ 0.27 mBq/kg, ^{238}U ≤ 0.25 mBq/kg, ^{226}Ra ≤ 0.37 mBq/kg and ^{210}Po = 1.41 mBq/kg (Table 1). This crystal was cut out from the Li_2MoO_4 bulk shown in Fig. 1. An exhaustive GDMS trace element chemical analysis was performed on every Li_2MoO_4 crystals that we grew, just below the seed, in the first stages of growth, in order to calculate the partition coefficients of impurities whenever it was possible. For the sake of clarity, we only present in Table 2 the results obtained for the crystal shown in Fig. 1. It turns out that the resulting Li_2MoO_4 crystal exhibits Fe, Cr, Ni, Co, Mn, Cu, Al, Li, Na, Ca, Mg contents lower than 1 ppm. What Table 2 shows is that the overall chemical purity of the crystal is outstanding.

Owing to the positive sign of k_0-*1* for all the impurities in Table 2, and especially for K and Fe, all impurities exhibit depletion in the melt which means that their concentration profile is concave with a higher value in the first stages of growth. Setting aside the W concentration (≈4 × 10^{17} cm^{-3}), all other impurity elements dissolved in the first growth stage of the Li_2MoO_4 crystal have a concentration lower than 10^{17} cm^{-3}. The iron content is quite low and that of Pt and Rh is undetectable. The partition coefficient of Fe is much closer to that of Al than to that of Co, which suggests that the iron is dissolved in the "3+" oxidation state instead of the "2+" one. The K and W impurities have a partition coefficient higher than 1, which might be due to homovalent $K_{Li}^{\times}$ and $W_{Mo}^{\times}$ substitutions. The W macro-depletion profile should remain relatively flat. The sign of all k_0-*1*-values deduced from Table 2 was cross-checked by complementary GDMS trace analysis on a piece of crystal extracted from the last stage of growth, and on a piece of the remaining growth load. Moreover, consistent results were obtained by these two methods, HPGe γ-spectroscopy and GDMS, in terms of ^{40}K-contamination and Ba/^{226}Ra correlation. The expected ^{40}K activity, deduced exclusively from the Li_2CO_3 and MoO_3 raw materials K-concentration obtained by GDMS analysis, in the as-grown crystals is ≈24.6 mBq/kg in the first stages of growth, typically in the first 5 mm below the seed, and ≈10.6 mBq/kg at 5 mm from the end of the bulk. According to the thermochemical data found in Refs. [35,36], the U_3O_8/UO_2 and MoO_3/MoO_2 reduction potentials are virtually superposed on each other for every temperature from room temperature to the melting temperature of Li_2MoO_4. U^{6+} cations are known to dissolve easily in many media (including in the form of UO_4^{2-} tetrahedra), but not U^{4+} and Th^{4+} cations. Unfortunately, it seems to be thermodynamically difficult to remove U^{6+} once it is caught in the

crystal since U^{4+} does not form without simultaneous reduction of Mo^{6+} to Mo^{4+}. Since the partition coefficient of W^{6+} or U^{6+} substituted for the lattice Mo^{6+} cations reads:

$$k_0 \approx e^{\left(\frac{\Delta S^s_{v,M} - \Delta S^l_{v,M}}{R}\right)} e^{\left[\frac{\Delta G_{m,Li2MO4} - \Delta G_{m,Li2MoO4} + \Delta H^l_{d,Li2MO4} - \Delta U_{lat} - 8\pi G r_{Mo}\left(r_M - r_{Mo}\right)^2}{RT}\right]}$$

where ΔS_v stands for vibrational entropy variation upon substituting M for Mo, ΔG_m for melting free energy variation of Li_2MO_4, ΔH_d for the dissolution enthalpy variation of Li_2MO_4 into Li_2MoO_4, ΔU_{lat} for the lattice energy variation upon substituting M for Mo, G for the Li_2MoO_4 average shear modulus, superscript "s" (resp. "l") for "in the solid (resp. liquid) state" and r for the relevant ionic radii, it might be inferred that the expected partition coefficient for U is higher than that of W (so > 1.12). The same kind of reasoning should hold for the respective partition coefficients of Ra^{2+} and Ba^{2+} (>1.28). If the former is already present in the starting powders, it should concentrate in the first stages of growth by depletion of the melt and so it should be necessary to cut the crystals in the second part of the crystalline bulk. This highlights the necessity in the future developments of purifying even the purest MoO_3 and Li_2CO_3 powders found on the market. The radiopurity of our crystals was found to be perfectly compatible with the final neutrino physics objective, even without purification of the initial Li_2CO_3 and MoO_3 powders, as far as the very dangerous contaminant ^{40}K is concerned. A too high activity in ^{40}K could give rise to random coincidences with other unavoidable events (for example those coming from the standard two-neutrino double-beta decay) that would produce background for 0v-DBD.

Fig. 5 shows a two-dimensional distribution of light-to-heat parameter (light yield) versus the detected heat. This scatter plot exhibits a prominent fully-populated band containing ß, γ and cosmic muon events.

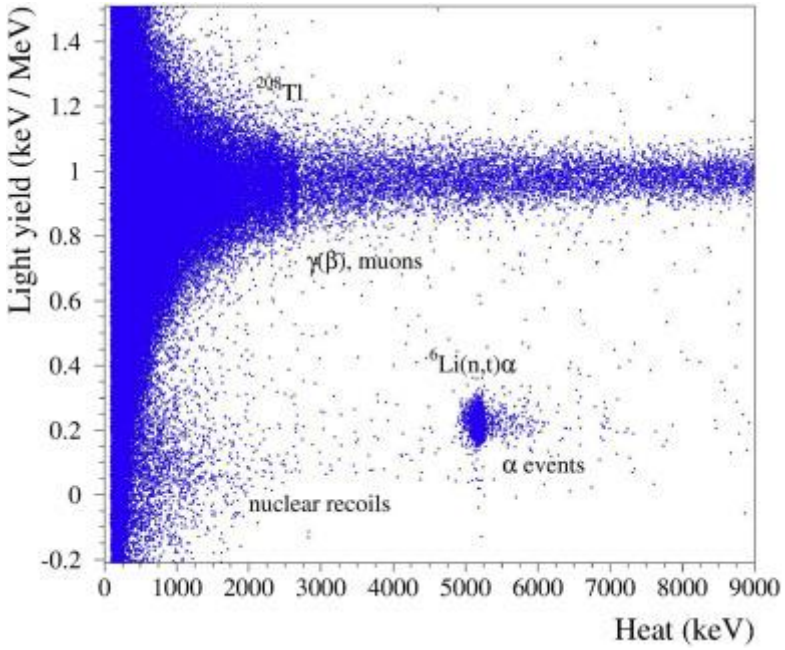

Fig. 5. Heat-scintillation discrimination diagram of a ~158 g Li_2MoO_4 crystal tested as a scintillating bolometer over 130.3 h of low-temperature measurements above ground.

The collected light yield related to this band is ≈0.95 keV/MeV at the energy of interest for 0v-DBD, i.e. ~3 MeV. A second salient feature of the scatter plot is a cloud of points with a much lower light emission with respect to the previous band. This class of events is due to neutron

absorption by ^{6}Li present at the level of 8% in nature and consequently in the tested Li_2MoO_4 crystal. ^{6}Li exhibits a very high cross section for thermal neutron capture (~940 b). This capture is followed by the emission of an α-particle and a tritium nucleus, releasing a total kinetic energy of 4.78 MeV. The collected light yield at the α-triton peak is ≈0.23 keV/MeV and the energy resolution (FWHM) on the capture n+^{6}Li amounted to 113 keV. The corresponding quenching factor of the mixed α-triton events with respect to ß/γ-events is about 0.24. Another structure observable in the scatter plot is a modestly populated band at low energies, whose events are due to nuclear recoils induced by fast neutrons scattering on elemental composition of the Li_2MoO_4 target. We remark that all the neutron-induced events detected by our device are due to the environmental background. No neutron source was used in these measurements. The potential of Li-containing scintillating bolometers for both thermal and fast neutron detection is obvious. There are several 0ν-DBD projects dedicated to the development of $ZnMoO_4$ (LUMINEU, LUCIFER) and of $CaMoO_4$ scintillating bolometers (AMoRE), and also preliminary tests on Li_2MoO_4 detectors [15,37], which are encouraging in spite of a light yield slightly lower than that observed in $ZnMoO_4$, on the order of $E_{light}/E_{heat} \sim 10^{-3}$. The advantages of Li_2MoO_4 are now obvious with respect to the other two ones: it contains 55% of Mo in weight, to be compared with 48% and 43% for Ca- and Zn-based compounds (although its lower density entails a few percent less molybdenum content by volume unit than in the other mentioned compounds), its melting temperature is several hundred degrees lower which reduces substantially volatilization and irrecoverable losses and subsequent parasitic intergrowths. Its space group exhibits a high symmetry which will permit to obtain more easily the growth orientation and control it by proper seeding preparation, as well as to achieve constant diameter and regular crystal shape (at least much more easily than in $ZnMoO_4$). Moreover, the lower melting entropy of Li_2MoO_4 crystals with respect to that of $ZnMoO_4$ crystals also avoids in the former the annoying faceting of the latter crystals, which also contributes to their irregular shapes. In addition, all the preliminary indications are in favor of the possibility to grow large mass crystals (Fig. 1). Many of its physical and physicochemical properties are known, including now their temperature dependencies, which makes this system amenable to advanced numerical simulations of the growth process aiming at upscaling the latter for the production foreseen in a one-ton experiment. In the perspective of an industrial production, to work at lower temperatures also decreases the contamination kinetics of the Pt crucibles to be used, and so enhances their life cycle. Last but not least, another advantage of Li_2MoO_4 crystals is their highest Debye temperature associated with zero-point energy, as compared to that of $ZnMoO_4$ and TeO_2 crystals (see discussion after, in Section 3.6.), as well as its lower refraction indexes [20].

Table 2
Results of the GDMS trace element analysis of the Czochralski grown Li_2MoO_4 single crystals displayed in Fig. 1. The relative error on the elements trace concentrations is on the order of 20%. The distribution coefficient was estimated with the GDMS analysis of the initial growth load.

Element	Below the seed: Content (ppm) Concentration (cm^{-3})	Last growth stage: Content (ppm) Concentration (cm^{-3})	Partition coefficient k_0
B	0.01 1.694×10^{15}	$\leq$0.01 $\leq 1.694 \times 10^{15}$	$\geq$1
Na	0.94 7.485×10^{16}	0.38 3.026×10^{16}	1.31
Mg	0.04 3.013×10^{15}	0.03 2.260×10^{15}	1.1
Al	0.37 2.51×10^{16}	0.09 6.105×10^{15}	1.49
Si	0.26 1.695×10^{16}	0.03 1.956×10^{15}	1.75
P	0.08 4.728×10^{15}	$\leq$0.01 $\leq 5.91 \times 10^{14}$	$\geq$1
S	1 5.71×10^{16}	0.5 2.855×10^{16}	1.24
Cl	0.04 2.066×10^{15}	0.03 1.550×10^{15}	1.1
K	0.55 2.575×10^{16}	0.21 9.832×10^{15}	1.33
Ca	0.6 2.741×10^{16}	$\leq$0.5 $\leq 2.284 \times 10^{16}$	$\geq$1
Ti	0.94 3.595×10^{16}	$\leq$0.5 $\leq 1.912 \times 10^{16}$	$\geq$1
Cr	0.08 2.817×10^{15}	$\leq$0.05 $\leq 1.760 \times 10^{15}$	$\geq$1
Fe	0.19 6.229×10^{15}	0.03 9.835×10^{14}	1.64
Co	0.006 1.864×10^{14}	0.006 1.864×10^{14}	$\approx$1
Ni	0.04 1.248×10^{15}	$\leq$0.01 $\leq 3.12 \times 10^{14}$	$\geq$1
Zn	0.49 1.372×10^{16}	$\leq$0.05 $\leq 1.4 \times 10^{15}$	$\geq$1
Rb	$\leq$0.003 $\leq 6.426 \times 10^{13}$	$\leq$0.005 $\leq 1.071 \times 10^{14}$	
Sr	0.06 1.254×10^{15}	0.003 6.27×10^{13}	2.04
Y	0.08 1.647×10^{15}	$\leq$0.05 $\leq 1.029 \times 10^{15}$	$\geq$1
Zr	0.06 1.204×10^{15}	$\leq$0.05 $\leq 1.003 \times 10^{15}$	$\geq$1
In	0.76 1.212×10^{16}	–	–
Cs	0.01 1.377×10^{14}	$\leq$0.005 $\leq 6.885 \times 10^{13}$	$\geq$1
Ba	0.56 7.465×10^{15}	0.25 3.333×10^{15}	1.28
W	40 3.983×10^{17}	28 2.788×10^{17}	1.12
Re	0.06 5.899×10^{14}	$\leq$0.05 $\leq 4.916 \times 10^{14}$	$\geq$1
Pt	$\leq$0.006 $\leq 5.631 \times 10^{13}$	$\leq$0.03 $\leq 2.815 \times 10^{14}$	
Tl	$\leq$0.002 $\leq 1.791 \times 10^{13}$	$\leq$0.005 $\leq 4.477 \times 10^{13}$	
Pb	$\leq$0.002 $\leq 1.767 \times 10^{13}$	$\leq$0.005 $\leq 4.417 \times 10^{13}$	
Bi	$\leq$0.002 $\leq 1.752 \times 10^{13}$	$\leq$0.005 $\leq 4.38 \times 10^{13}$	
Th	$\leq$0.0003 $\leq 2.367 \times 10^{12}$	$\leq$0.0008 $\leq 6.312 \times 10^{12}$	
U	$\leq$0.0004 $\leq 3.076 \times 10^{12}$	$\leq$0.001 $\leq 7.69 \times 10^{12}$	
Ra	$\leq$0.0005 $\leq 4.05 \times 10^{12}$	$\leq$0.001 $\leq 8.1 \times 10^{12}$	

Pd, Ag, Sn, Sb, I $< 9 \times 10^{16}$ cm^{-3}
F, Nb, Ru, Rh, Te, La, Ce, Hg $< 10^{16}$ cm^{-3}
Be, Sc, V, Cu, Ga, Se, Br, Hf, Ir $< 4 \times 10^{15}$ cm^{-3}
Mn, Ge, As, Pr, Nd, Sm, Eu, Gd, Tb, Dy, Ho, Er, Tm, Yb, Lu, Os $< 7 \times 10^{14}$ cm^{-3}

3.5. Exploratory crystal growth of $Li_4Mo_5O_{17}$

In this section we report our first results related to the growth and the investigation of some properties of $Li_4Mo_5O_{17}$, which were triggered by the following question, interesting from the 0v-DBD point of view: is it possible to grow lithium molybdate crystals which exhibit a congruent melting point at a lower temperature than the melting temperature of Li_2MoO_4, a higher Mo weight % and a higher density? According to all existing Li_2O-MoO_3 pseudobinary phase diagrams, there is such a phase corresponding to the chemical composition $Li_4Mo_5O_{17}$ with congruent T_m = 544 °C [38], congruent T_m = 560 °C [39], almost uncongruent $T_{m/p}$ = 547 °C [40], or $Li_2Mo_2O_7$ with congruent T_m = 535 °C [41]. There is also another phase corresponding to the chemical composition $Li_2Mo_4O_{13}$ with almost uncongruent $T_{m/p}$ = 568 °C [38], uncongruent T_p = 576 °C [41], more strongly uncongruent T_p = 580 °C and undergoing a crystallographic phase transition at T_t = 550 °C [39], or almost uncongruent $T_{m/p}$ = 570 °C [40]. It turns out that $Li_4Mo_5O_{17}$ contains 61.5% in Mo weight and has a room temperature density of 4.18 g/cm^3, both characteristics being higher than in Li_2MoO_4 (55% Mo wt and 3.04 g/cm^3, respectively). Fig. 6 shows the first results we could get by static solidification: transparent and colourless millimeter-sized single crystals in the first stages of growth turning to yellow and finally brown and opaque crystals in the subsequent stages of growth. The yellow colour remained unaffected by post-growth thermal annealing near the melting point under O_2 atmosphere. Powder XRD as a function of solidification distance showed no phase evolution and the lattice parameters found by fitting the XRD pattern of transparent and brown samples were virtually the same ($P\bar{1}$, a = 6.7771 Å, b = 9.4709 Å, c = 10.8047 Å, α = 73.15°, ß = 88.96°, γ = 69.77°, R_{wp} = 15, x^2 = 2.31). The crystallographic model is the one described in Ref. [42], with $[Mo_5O_{17}]$ infinite ribbons propagating along ***b***, held together by $Li(1)O_4$ and $Li(2)O_4$ tetrahedra and $Li(3)O_6$ and $Li(4)O_6$ octahedra. The Inductively Coupled Plasma/Atomic Emission Spectroscopy chemical analysis of Li and Mo contents in the colourless and the brownish crystals showed differences lying within the error bar, so that no clear conclusions could be induced. If there is a solid solution of the $Li_{4+x}Mo_5O_{17}$ type, then what our results suggest is that the Li content does not vary enough over the temperature range ($\Delta T_r \sim 20$ °C) between the $Li_4Mo_5O_{17}$ peritectic decomposition plateau and the Li_2MoO_4-$Li_4Mo_5O_{17}$ eutectic plateau.

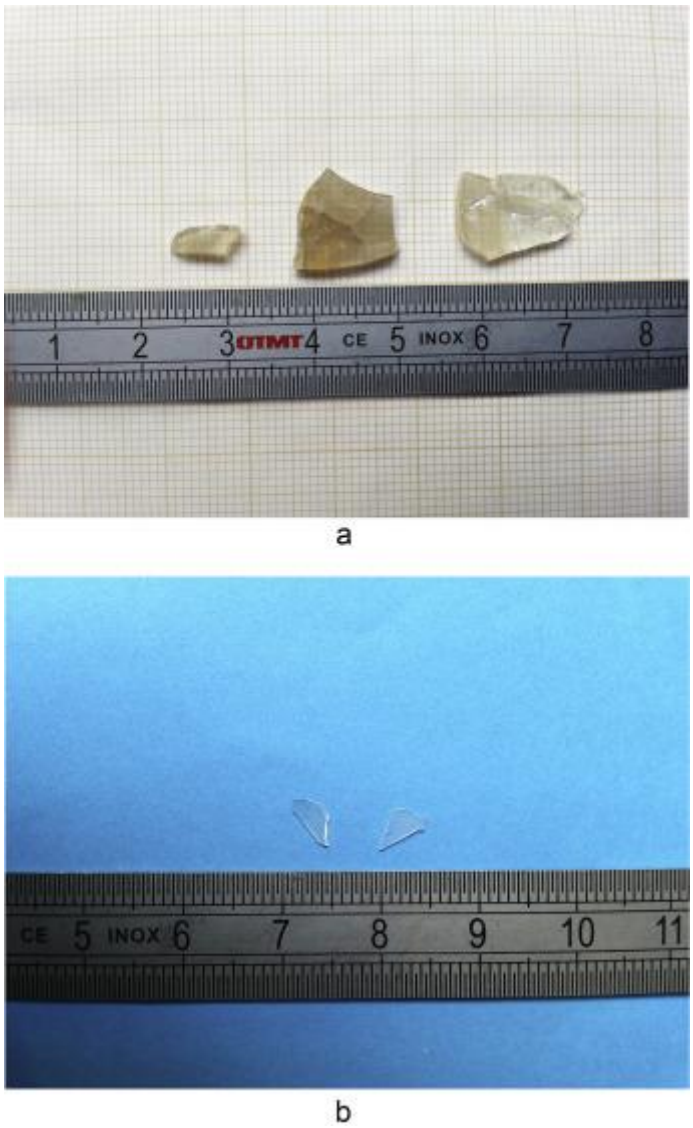

Fig. 6. Second attempt at growing $Li_4Mo_5O_{17}$: very small colourless and transparent crystals.

However, we did observe a specific feature in the brown crystals by DSC. Indeed, in the brown crystals a first-order phase transition was observed, with T_t = (755.1 ± 1.0) K, ΔH_t = (1442.1 ± 57.7) J/mol and ΔS_t = (0.23 ± 0.01) R. The temperature variation rate did not impact T_t, but it did impact the range of hysteresis upon cooling, ΔT_h going from −29.2 °C at −3 °C/mn to −44.4 °C at −20 °C/mn. The difference between the melting latent heat of the $Li_4Mo_5O_{17}$ colourless and brown crystals is ~6 times higher than the phase transition latent heat observed in the brown $Li_4Mo_5O_{17}$ crystals. Hence, the phase transition has probably nothing to do with the melting mechanism in $Li_4Mo_5O_{17}$. The melting temperature, enthalpy and entropy of the colourless (resp. brown) $Li_4Mo_5O_{17}$ crystal was found to be T_m = (819.4 ± 1.0) K (resp. 818.5 ± 1.0 K), ΔH_t = (185.83 ± 7.43) kJ/mol (resp. 176.21 ± 7.05 kJ/mol) and ΔS_t = (27.3 ± 1.1) R (resp. 25.9 ± 1.0 K). As can be seen in the upper inset of Fig. 7,

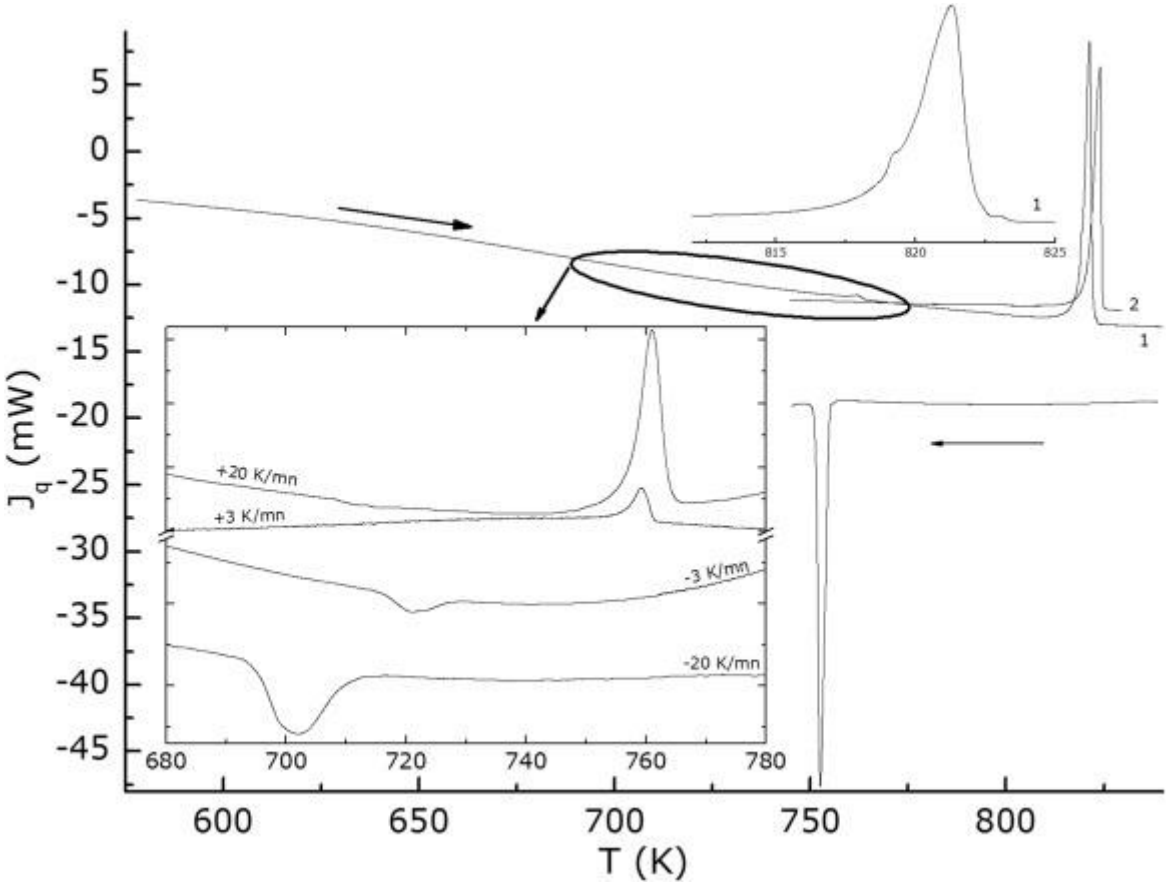

Fig. 7. Differential scanning calorimetry of brown $Li_4Mo_5O_{17}$ sample. The lower inset shows temperature cycles around the phase transition starting at 482 °C. The upper inset displays a focus on the melting peak at the first heating run (curve 1) and at the second heating run (curve 2).

the melting peak is highly structured. In colourless $Li_4Mo_5O_{17}$, there is first a deviation from the baseline which starts at 817.8 K, and then there is a shouldering of the main peak at 819 K. In brown $Li_4Mo_5O_{17}$, we do not observe the deviation from the baseline, but we also see the shouldering at 817.1 K. Both crystals exhibit a doubled and broad solidification peak upon cooling with onset temperatures ~750.7–754.4 K. Upon re-heating the sample, we observe a different melting peak, broad but single, at 821.4 K for the colourless sample, and 819.3 K for the brown one. This significant shift and change of nature of the melting peak is a strong indication of an uncongruent melting behavior. In the brown $Li_4Mo_5O_{17}$ sample, the phase transition peak can be seen only during the first heating stage, and no longer after the melting-solidification cycle. The melting peak obtained after a third heating stage did not show any significant change with respect to that obtained after the second heating stage. We completed this thermal analysis by powder X-ray diffraction on the products obtained after the first cooling, and after the second cooling. Contrary to the initial powder, which was pure brown $Li_4Mo_5O_{17}$ compound, the single- and twice-melted powders were found to be a mixture of $Li_4Mo_5O_{17}$ phase, and of a high-temperature and a low-temperature form of $Li_2Mo_4O_{13}$ (both triclinic P-1) [40]. Noticeably, the height over which single crystals (either colourless or brown) could be grown compares favourably to $\Delta T_r/|\nabla T| \approx 10$ mm (with $|\nabla T| \approx 20$ °C/cm).

Transmission measurements performed over a 1.64 mm-thick colourless and transparent crystal to the naked eye led to an uncorrected absorption coefficient of ~3.5 cm^{-1} at 590 nm. Even if the Sellmeier equations for the optical indexes of this compound are not already known, we can safely

put that this value is clearly well above the crystal specifications for a ton-scale 0v-DBD experiment (≈0.033 cm^{-1} over the 550–700 nm spectral range).

3.6. Specific heat and Debye temperature trends in HSCB crystals

Li_2MoO_4 specific heat and Debye temperature were compared to those of $^{6}Li_6Eu(^{10}BO_3)_3$, a crystal which we develop for fast neutron detection applications [26], of $ZnMoO_4$ and TeO_2, two well-known crystals in the DBD searches, and of $Li_4Mo_5O_{17}$ discussed in the previous section and measured here for the first time. In particular, the CUORE experiment located in the LNGS in Italy will hold soon 988 TeO_2 crystals of 750 g each in one cryostat representing a real ton-scale 0v-DBD cryogenic experiment, however exploiting only heat and not heat-light bolometric technology.

Neither Schottky peak nor long range ordering was observed in $Li_4Mo_5O_{17}$, either transparent or brown, nor in Li_2MoO_4 down to 2 K on the specific heat measurement (Fig. 8), which is important if several hundred kg of crystals are to be cooled at cryogenic temperatures in the context of a 0v-DBD experiment. The specific heat could be approximated for temperatures higher than ~50 K by means of high-temperature series expansion (formula (5) of Ref. [43] and red curve in Fig. 8), which yielded a high Debye temperature of θ_D = 759.1 K and the following Bernoulli numbers: B_1 = −2.01553, B_2 = 2.00385, B_3 = −0.9918, B_4 = 0.00152, for Li_2MoO_4. Such a high value of the Debye temperature is excellent for HSCB operation since at very low temperatures, typically a few tens of mK, heat is carried through the crystal lattice by the scarce acoustic phonon modes that are still populated.

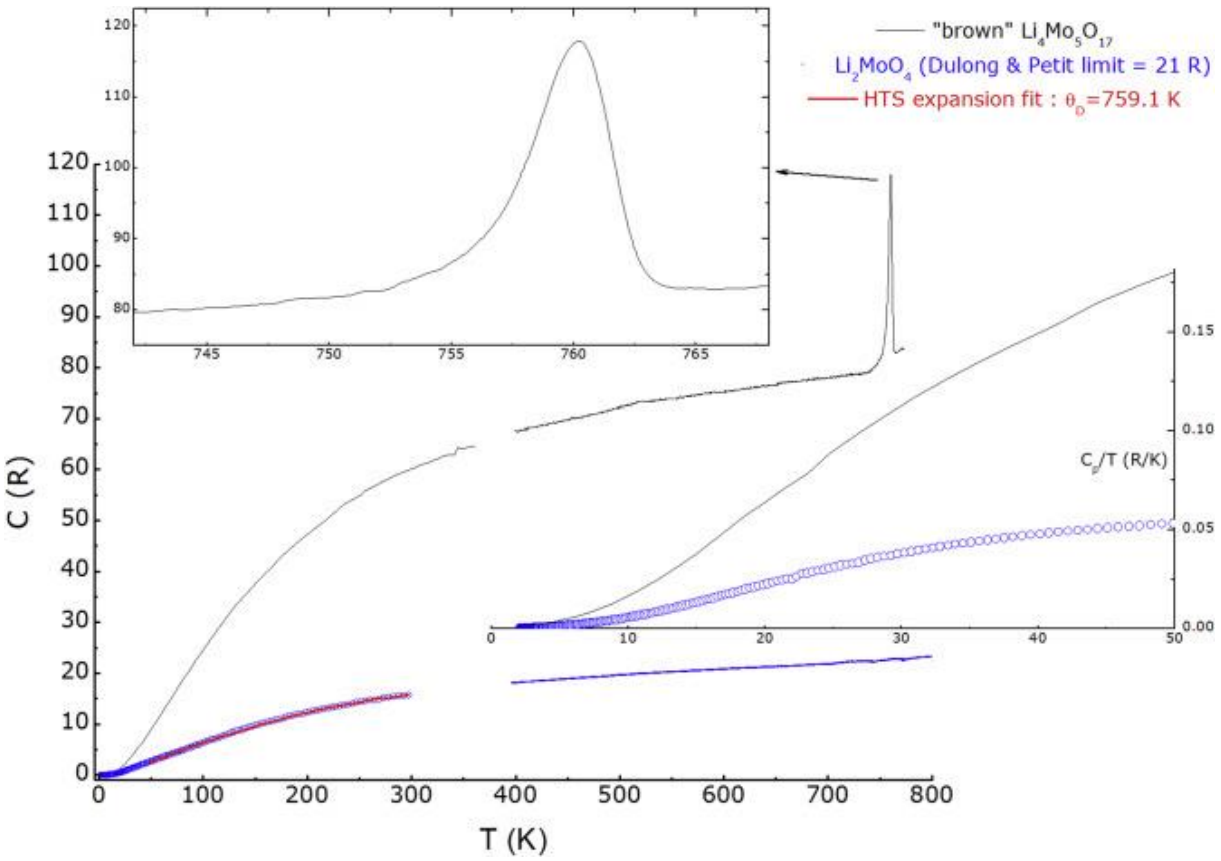

Fig. 8. Specific heat in R units versus temperature curve of a colourless Li_2MoO_4 single crystal and of brown $Li_4Mo_5O_{17}$ crystal. The lower inset shows the C_p/T function in both compounds at low temperatures, and the upper one a focus on the first-order phase transition in brown $Li_4Mo_5O_{17}$.

Fig. 9 shows the normalized phononic contribution to the specific heat as a function of temperature in several crystals investigated and developed for rare events searches with bolometric technology. In all of them, $C_p/3NR$ at 350 K reaches ~0.8 to the maximum, which stands well below the Dulong & Petit limit and suggests that low anharmonic effects are at play at this temperature, consistently with the high θ_D obtained by the high-temperature series expansion fit. On such a graph, the deviation from the Dulong & Petit limit is expected to increase with the strength of interatomic forces and the lightness of the atoms. The zero-point energy and the Debye temperature are proportional to the area between the $C_{ph}/3NR = 1$ line (Dulong & Petit limit) and the actual $C_{ph}/3NR$ curve. Hence, integrating the data for all crystals between 4 and 297 K, and calibrating the area with the θ_D-values of LiF and α-Al_2O_3 crystals, one obtains the following θ_D-trend in this series: $\theta_D(^6Li_6Eu(^{10}BO_3)_3) \approx 910$ K > $\theta_D(Li_2MoO_4) \approx 765$ K > $\theta_D(Li_4Mo_5O_{17}) \approx 669$ K > $\theta_D(TeO_2) \approx 641$ K > $\theta_D(ZnMoO_4) \approx 616$ K. The values found by this procedure, which really relates the Debye temperature to the zero-point energy, are in very good agreement (better than 4.3% for all crystals) with the values obtained by the high-temperature series expansion fits of the data at high temperature. Consequently, it turns out that from the very low temperature thermal transport viewpoint, Li_2MoO_4 has better potential than TeO_2 and $ZnMoO_4$ for 0ν-DBD decay searches exploiting cryogenic particle detectors.

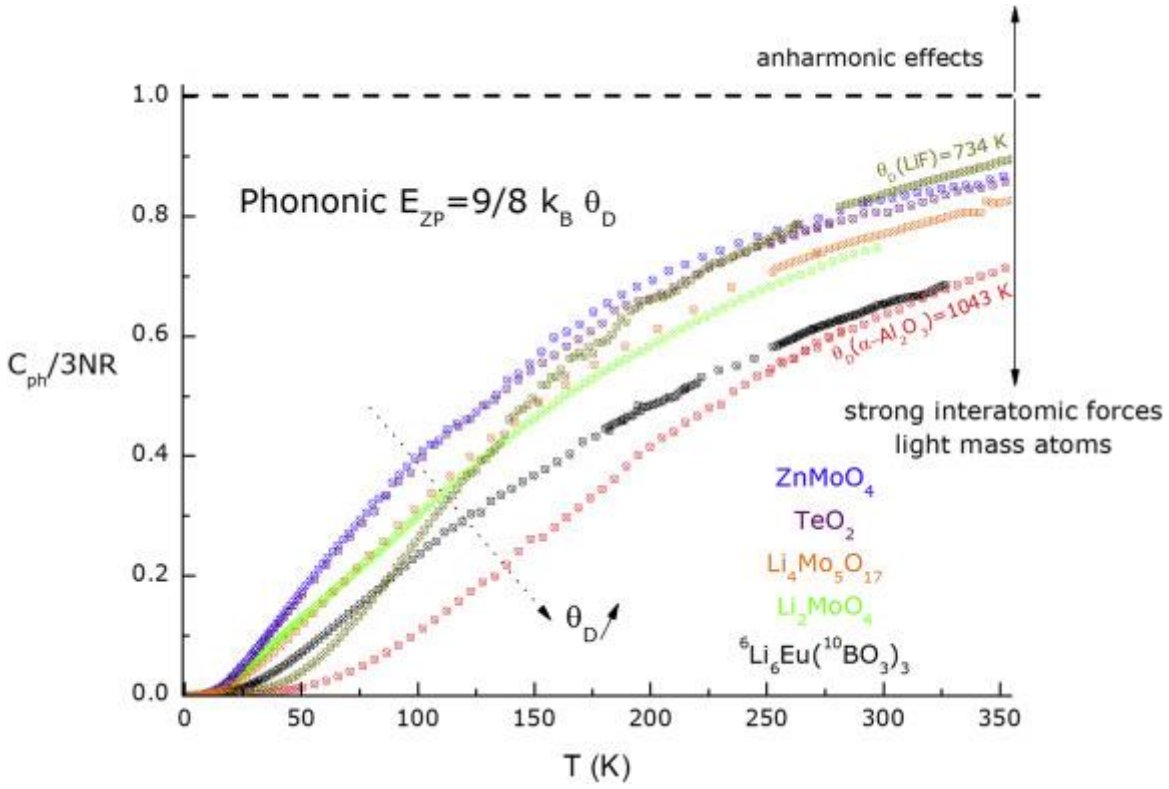

Fig. 9. Normalized phononic contribution to the specific heat as a function of temperature in several crystals investigated and developed for bolometric rare events searches.

4. Conclusions

We have successfully grown 230 g Li_2MoO_4 single crystals by the Czochralski method in a Pt crucible under air atmosphere. The crystals' characterization demonstrates their promising properties for

HSCB operation in terms of radiopurity levels ($^{40}K \leq 47$ mBq/kg, $^{226}Ra \leq 0.37$ mBq/kg, $^{232}Th \leq 0.21$ mBq/kg, $^{228}Th \leq 0.27$ mBq/kg), optical transmission ($\alpha_{corr}(589\ nm) = 0.05\ cm^{-1}$) and thermal properties ($\theta_D \approx 765$ K, no phase transition down to 2 K). The thermal expansion, dilatometric and calorimetric analysis partly explains why these crystals are much easier to grow than other molybdates being developed for such applications, especially $ZnMoO_4$. All the impurities partition coefficients in Li_2MoO_4 were found to be higher than 1, and the resulting melt depletion was confirmed by all the impurities concentration measurements performed in the last stage of growth. Bolometer operation demonstrated that β, γ and cosmic muon events can be discriminated, as well as α events arising from the $^6Li(n,t)\alpha$ reaction. Finally, we grew small size $Li_4Mo_5O_{17}$ crystals and characterized their specific heat and Debye temperature ($\theta_D \approx 669$ K). High mass and optical grade $Li_4Mo_5O_{17}$ crystals could be grown in the future provided their slightly uncongruently melting behavior can be dealt with.

Acknowledgements

We thank Vladimir Shlegel for lending us the $ZnMoO_4$ single crystal used for specific heat measurement and Thierry Redon for the many cutting and polishing of the Li_2MoO_4 crystals. MV would also like to thank Fedor Danevich, Vladimir Tretyak and Roman Boiko for relevant and clever comments. ANR agency (n°ANR 12-BS05-004-04) is acknowledged for funding the LUMINEU project.

References

1. M. Tenconi, *et al.* Phys. Procedia, 61 (2015), pp. 782-786.
2. G. Angloher, *et al.* Phys. Dark Univ., 3 (2014), pp. 41-74.
3. A.V. Derbin, *et al.* Eur. Phys. J. C, 74 (2014), p. 3035
4. E. Armengaud, *et al.* J. Cosmol. Astropart. Phys., 2013 (November 2013)
5. L. Pattavina, LUCIFER collaboration EPJ Web Conf., 65 (2014), p. 02003
6. R.D. Peccei, H.R. Quinn hys. Rev. Lett., 38 (1977), p. 1440
7. Gonzalez-Mestres, L., Perret-Gallix, D., Proceedings of the 2nd European Workshop on Low Temperature Devices for the Detection of Low Energy Neutrinos and Dark Matter, Annecy, France, May 2–4, 1–36 (1988).
8. L. Gonzalez-Mestres. **Proceedings of the 2nd international workshop on theoretical and phenomenological aspects of underground physics, toledo (Spain), September 1991** Nucl. Phys. B Proc. Suppl., 28A (1992), pp. 478-481.
9. L. Cardani, *et al.* JINST, 7 (2012), p. P01020.
10. D.M. Chernyak, *et al.* Eur. Phys. J. C, 72 (2012), p. 1989.
11. O.P. Barinova, *et al.* Nucl. Instrum. Meth. Phys. Res. A, 613 (2010), p. 54.
12. Barinova, Olga, et al., Poster Presentation at the 17th International Conference on Crystal Growth and Epitaxy, Warsaw, Poland, August 2013, 11–16.
13. O.P. Barinova, *et al.* Nucl. Instrum. Meth. Phys. Res. A, 607 (2009), p. 573.
14. O.P. Barinova, *et al.* J. Cryst. Growth, 401 (2014), p. 853.
15. T.B. Bekker, N. Coron, F.A. Danevich, V. Ya. Degoda, A. Giuliani, V.D. Grigorieva, N.V. Ivannikova, M. Mancuso, P. de Marcillac, I.M. Moroz, C. Nones, E. Olivieri, G. Pessina, D.V. Poda, V.N. Shlegel, V.I. Tretyak, M. Velazquez. Astropart. Phys., 72 (2016), pp. 38-45.
16. D. Elwell, H.J. Scheel. Crystal Growth from High-temperature Solutions, Academic Press (1975).
17. E. Takayama-Muromachi, A. Navrotsky, S. Yamaoka. J. Sol. St. Chem., 65 (1986), pp. 241-250.
18. V.N. Shlegel, L. Berge, R.S. Boiko, M. Chapellier, D.M. Chernyak, N. Coron, F.A. Danevich, R. Decourt, V. Ya. Degoda, L. Devoyon, A. Drillien, L. Dumoulin, C. Enss, A. Fleischmann, L. Gastaldo, A. Giuliani, M. Gros, S.

Herve, I.M. Ivanov, V.V. Kobychev, Ya. P. Kogut, F. Koskas, M. Loidl, P. Magnier, E.P. Makarov, M. Mancuso, P. de Marcillac, S. Marnieros, C. Marrache-Kikuchi, S.G. Nasonov, X.F. Navick, C. Nones, E. Olivieri, B. Paul, Y. Penichot, G. Pessina, O. Plantevin, D.V. Poda, T. Redon, M. Rodrigues, O. Strazzer, M. Tenconi, L. Torres, V.I. Tretyak, Ya. V. Vasiliev, M. Velazquez, O. Viraphong, V.N. Zhdankov **Proceedings of the 3rd RPScint "Radiopure scintillators" workshop** Eur. Phys. J. Web Conf., 65 (03001) (2014), pp. 1-6.

19. E. Bellotti, C. Broggini, G. Di Carlo, M. Laubenstein, R. Menegazzo. Phys. Lett. B, 710 (2012), pp. 114-117.
20. B. Ph. Bilenkii, M.V. Markiv, I.D. Tretyak. Fiz. Elektron. Lvov, 8 (1974), pp. 94-95.
21. U. Kolitsch. Z. Kristal., 216 (2001), pp. 449-454.
22. M. Velázquez, A. Ferrier, J.-P. Chaminade, B. Menaert, R. Moncorgé. J. Cryst. Growth, 286 (2) (2006), pp. 324-333.
23. A. Ferrier, M. Velázquez, X. Portier, J.-L. Doualan, R. Moncorgé. J. Cryst. Growth, 289 (1) (2006), pp. 357-365.
24. A. Ferrier, M. Velázquez, O. Pérez, D. Grebille, X. Portier, R. Moncorgé. J. Cryst. Growth, 291 (2) (2006), pp. 375-384.
25. Hassan El Hafid, Matias Velázquez, Olivier Pérez, Abdelaziz El Jazouli, Alain Pautrat, Rodolphe Decourt, Emmanuel Véron, Oudomsack Viraphong, Claude Delmas. J. Sol. St. Chem., 202 (2013), pp. 85-92.
26. Rekia Belhoucif, Matias Velázquez, Yannick Petit, Olivier Pérez, Benoît Glorieux, Oudomsack Viraphong, Pierre de Marcillac, Noël Coron, Lidia Torres, Emmanuel Véron, AbdelHamid Kellou, Philippe Veber, Rodolphe Decourt, Hassan El Hafid. CrystEngComm, 15 (2013), pp. 3785-3792.
27. Elias Castel, Philippe Veber, Marjorie Albino, Matias Velázquez, Stanislas Péchev, Dominique Denux, Jean-Pierre Chaminade, Mario Maglione, Michaël Josse. J. Cryst. Growth, 340 (2012), pp. 156-165.
28. F.A. Danevich, *et al.* Nucl. Phys. A, 694 (2001), p. 375.
29. P. Belli, *et al.* Nucl. Instr. Meth. A, 498 (2003), p. 352.
30. R. Bernabei, *et al.* AIP Conf. Proc., 1549 (2013), p. 189.
31. P. Belli, *et al.* Eur. Phys. J. A, 50 (2014), p. 134.
32. P. Belli, *et al.* Nucl. Phys. A, 789 (2007), p. 15.
33. F.A. Danevich, *et al.* Nucl. Instrum. Meth. A, 631 (2011), p. 44.
34. A.N. Annenkov, *et al.* Nucl. Instr. Meth. A, 584 (2008), p. 334.
35. (second ed.)O. Knacke, O. Kubaschewski, K. Hesselmann (Eds.), Thermochemical Properties of Inorganic Substances, vols. 1 and 2, Springer, Berlin, Heidelberg, New York (1991)
36. I. Barin, G. Platzki. Thermochemical Data of Pure Substances, vol. II (La-Zr) (third ed.), VCH, Weinheim, New York, Basel, Cambridge, Tokyo (1995).
37. L. Cardani, *et al.* JINST, 8 (2013), p. P10002.
38. W.S. Brower, *et al.* J. Cryst. Growth, 16 (2) (1972), pp. 115-120.
39. S.F. Solodovnikov, *et al.* Zh. Neorg. Khim., 44 (6) (1999), pp. 1016-1023.
40. M. Moser, *et al.* Cryst. Res. Technol., 43 (4) (2008), pp. 350-354.
41. M. Parmentier, *et al.* Bull. Soc. Chim. Fr., 5 (1972), pp. 1743-1746.
42. M. Wiesmann, *et al.* Zeit. Kristal., 212 (1997), pp. 795-800.
43. J.E. Gordon, M.L. Tan, R.A. Fisher, N.E. Phillips, Sol. St. Comm., 69 (6) (1989), pp. 625-629.